Research Square

Preprints are preliminary reports that have not undergone peer review.
They should not be considered conclusive, used to inform clinical practice,
or referenced by the media as validated information.

Assessing the average maximum failure probability of unsaturated slopes over a given exposure period under stochastic rainfall

Shunchuan Wu
University of Science and Technology Beijing
Beibei Sun
University of Science and Technology Beijing
Longqiang Han
lqhan2014@163.com
Kunming University of Science and Technology https://orcid.org/0000-0002-6493-4115
Qiang Zhu
Suzhou SINOMA Design and Research Institute of Non-metallic Minerals Industry Co. Ltd.
Chaoqun Chu
University of Science and Technology Beijing

Research Article

Keywords: Average maximum failure probability (AMFP), Exposure period, Stochastic rainfall, Surrogate model, Unsaturated slope

Posted Date: April 8th, 2026

DOI: https://doi.org/10.21203/rs.3.rs-8982869/v1

License: This work is licensed under a Creative Commons Attribution 4.0 International License.
Read Full License

Version of Record: A version of this preprint was published at Natural Hazards on October 30th, 2026.
See the published version at https://doi.org/10.1007/s11069-026-08488-w.

Assessing the average maximum failure probability of unsaturated slopes over a given exposure period under stochastic rainfall

Authors

Shunchuan Wu [a, b, c, d, e], Beibei Sun [a, b], Longqiang Han [c, d, e, *], Qiang Zhu [f], Chaoqun Chu [a, b]

Affiliations

[a] *School of Resources and Safety Engineering, University of Science and Technology Beijing, Beijing 100083, China*

[b] *Key Laboratory of Ministry of Education for Efficient Mining and Safety of Metal Mines,USTB, Beijing 100083, China*

[c] *School of Land Resources Engineering, Kunming University of Science and Technology, Kunming 650093, China*

[d] *Key Laboratory of Geohazard Forecast and Geoecological Restoration in Plateau Mountainous Area, Ministry of Natural Resources of the People's Republic of China, Kunming 650093, China*

[e] *Yunnan Key Laboratory of Geohazard Forecast and Geoecological Restoration in Plateau Mountainous Area, Kunming 650093, China*

[f] *Suzhou SINOMA Design and Research Institute of Non-metallic Minerals Industry Co. Ltd., Suzhou 215000, China*

[*] Corresponding author

E-mail addresses: lqhan2014@163.com (Longqiang Han)

Abstract： Rainfall-induced landslides pose a significant threat to infrastructure and safety. Traditional deterministic approaches and many probabilistic methods are limited in their ability to evaluate the cumulative risk induced by multiple rainfall events over a specified time horizon. This study proposes a novel probabilistic framework to assess the average maximum failure probability (AMFP) of unsaturated soil slopes over a given exposure period (T) under multiple stochastic rainfall. The framework integrates rainfall randomness, geotechnical uncertainty, and unsaturated hydro–mechanical coupling, while addressing key challenges related to exposure-period aggregation and computational efficiency. The dependence structure between rainfall duration and intensity, including long-tail characteristics of extremes, is modeled using a Frank Copula based on historical rainfall data. Coupled seepage–stability simulations are implemented in FLAC3D through customized FISH scripting. To enable large-scale Monte Carlo analysis, a high-accuracy Support Vector Regression (SVR) surrogate model is constructed to replace computationally expensive numerical simulations. Application to a homogeneous slope in Baotou, China, indicates that the AMFP increases monotonically with exposure duration, rising from 2.52% (T=0.5 year) to 3.08% (T=5 years), demonstrating cumulative amplification of failure risk under stochastic rainfall. For T=1 year (34 rainfall events), the AMFP is 2.69%, corresponding to a reliability index of 1.927. Sensitivity analysis shows that rainfall duration and intensity exert comparable influences on failure probability, while soil strength parameters remain the dominant controlling factors. By linking stochastic rainfall occurrence with exposure-period-based extreme response, the proposed framework provides a rigorous and computationally efficient tool for time-dependent slope reliability assessment and risk-informed engineering decision-making.

Keywords: Average maximum failure probability (AMFP), Exposure period, Stochastic rainfall, Surrogate model, Unsaturated slope

Highlights

- Proposes the average maximum failure probability (AMFP) to quantify slope failure risk over a specified exposure period under multiple stochastic rainfall events.
- Establishes an exposure-period-based extreme aggregation framework that links sequential rainfall events with time-dependent reliability assessment.
- Integrates Frank Copula-based rainfall modeling with unsaturated seepage–stability simulations in FLAC3D using customized FISH scripting.
- Develops a high-accuracy SVR surrogate model to enable efficient large-scale Monte Carlo estimation of AMFP.
- Demonstrates monotonic amplification of failure probability with increasing exposure duration, highlighting the importance of time-scale consideration in slope risk evaluation.

Nomenclature

Nomenclature	Full Name	Description
AMFP	Average maximum failure probability	An indicator used to evaluate the instability risk of slopes affected by rainfall during a given exposure period
FOS	Factor of Safety	Ratio of resisting force to driving force
SWCC	Soil–water characteristic curve	Function describing the dependence of volumetric water content (or effective saturation) on matric suction
HCF	Hydraulic conductivity function	Function describing the variation of unsaturated hydraulic conductivity with effective saturation
SVR	Support Vector Regression	Regression version of support vector machine
MLE	Maximum Likelihood Estimation	Statistical method for estimating optimal model
IETD	Inter-Event Time Definition	Minimum time interval separating independent rainfall events
CV	Coefficient of Variation	Ratio of standard deviation to mean, indicating relative variability
PDF	probability density function	Likelihood function of a continuous variable
CDF	cumulative distribution function	Cumulative probability function of a continuous variable
R^2	Coefficient of Determination	Metric for model fit quality
RMSE	Root Mean Squared Error	Metric for model prediction accuracy
MAE	Mean Absolute Error	Metric for the average absolute error
GPD	Generalized Pareto Distribution	Continuous probability distributions used for modeling random variables
LogN	Lognormal Distribution	
Normal	Normal Distribution	
Exp	Exponential Distribution	
GEV	Generalized Extreme Value Distribution	

1. Introduction

Climate change and expanding human activities are contributing to a notable increase in the frequency and magnitude of slope failures and landslides, making them the second most significant geological hazard after earthquakes(Wu et al. 2024). It is well established that rainfall is a key triggering factor for slope instability (Bai et al. 2022; Shi et al. 2020; Wang and Xu 2025; Yan et al. 2023; Zhang et al. 2016), with rainfall-induced landslides accounting for approximately 90% of the total landslides worldwide (Haque et al. 2016; Wang et al. 2018). Consequently, developing scientifically robust methods for slope stability and risk assessment under rainfall infiltration is of critical theoretical and practical importance. The core challenge, however, lies not in understanding the physical mechanism—which is well-known—but in reliably quantifying the associated risks.

The mechanism is clear: infiltrating rainwater reduces matric suction (negative pore water pressure) in the unsaturated soil zone, which in turn diminishes the soil's shear strength—this is recognized as the primary driver of instability(Alsubal et al. 2019; Liu et al. 2021; Ran et al. 2018; Zhou et al. 2021). Thus, the central task shifts to developing predictive and quantitative assessment methods that can account for this process in the face of inherent uncertainties.

Traditional deterministic methods for slope stability analysis treat geotechnical parameters and external loads as fixed values and adopts the factor of safety (FOS) as the sole evaluation index (Reale et al. 2015). However, geotechnical parameters such as cohesion and friction angle exhibit substantial uncertainty due to geological variability (Wu et al. 2019), while rainfall intensity and duration are highly random in nature (Liu and Wang 2023; Tang et al. 2018). Deterministic analyses cannot explicitly quantify these uncertainties, which may lead to overly conservative or unsafe assessments and fail to realistically reflect the dynamic response and failure risk of slopes subjected to stochastic rainfall. To address these limitations, probabilistic and uncertainty-based methods have been increasingly adopted in geotechnical engineering. Techniques such as Monte Carlo simulation (MCS) (Li et al. 2013; Ma et al. 2017; Wu et al. 2019), random finite element (RFE) (Fang et al. 2024; Jiang et al. 2014), random finite difference (RFD), random limit equilibrium (RLE) (Yazdi and Moss 2025), Bayesian updating (Liu and Wang 2021), subset simulation (Zhang et al. 2025), and Copula functions (Jun et al. 2017) have been widely employed to quantify slope failure probability, providing a more rigorous foundation for landslide risk assessment.

Probability analysis of rainfall-induced slope instability must simultaneously account for uncertainties in both rainfall and geotechnical parameters (Zhang et al. 2025). While uncertainties in geotechnical parameters can be reasonably estimated through statistical analysis of laboratory or in situ test data, rainfall exhibits strong spatiotemporal variability, and extreme rainfall events—though rare—play a critical role in slope failures. This makes the statistical characterization and stable fitting of rainfall distributions especially challenging (Liu and Wang 2021). Moreover, when probabilistic

methods are applied to unsaturated slopes under rainfall infiltration, a major challenge arises from computational cost: unsaturated hydro-mechanical coupled numerical simulations are computationally expensive, performing tens of thousands of simulations—as required by Monte Carlo or related methods—results in an extremely high computational burden (Zhang et al. 2025).

Although significant progress has been made in probabilistic slope reliability analysis under rainfall conditions, most existing studies focus on single-event failure probability. In contrast, exposure-period-based extreme aggregation of sequential rainfall events has rarely been explicitly formulated for unsaturated slopes, limiting the ability to evaluate cumulative risk over a specified service period. To overcome the above challenges, this study proposes a novel and computationally efficient probabilistic framework. The core contributions of this study are threefold: (1) It proposes the concept of average maximum failure probability (AMFP) to quantify the integrated risk over a specified exposure period T, directly addressing the need for multi-event risk assessment. (2) It develops a high-accuracy Support Vector Regression (SVR) surrogate model to bypass the computational bottleneck, enabling efficient probabilistic analysis. (3) It employs a Frank Copula function to rigorously construct the joint probability model of rainfall intensity and duration, capturing both dependence and extreme characteristics. The proposed framework is implemented and validated through a detailed case study of a homogeneous soil slope in Baotou, China.

The remainder of this paper is organized as follows: Chapter 2 reviews the theoretical foundations, including unsaturated seepage, shear strength of unsaturated geomaterials, the strength reduction method, and probabilistic indicators such as failure probability and reliability index. Chapter 3 details the procedure for assessing the average maximum failure probability of unsaturated slopes over a given exposure period under stochastic rainfall. Chapter 4 presents the case study, covering model setup, validation, and the probabilistic assessment results. Section 4 presents a discussion of key findings and their implications. Section 5 provides the main conclusions.

2. Theoretical background

2.1. Unsaturated seepage

In unsaturated geomaterials, matric suction (negative pore water pressure) commonly exists and represents the most distinctive feature differentiating unsaturated flow from saturated flow. Matric suction is a key indicator governing the infiltration behavior of unsaturated soils and is closely related to the volumetric water content or saturation, both of which are typically characterized by the soil–water characteristic curve (SWCC) (Fredlund 2021). The relationship between volumetric water content and matric suction can be described by the Van Genuchten model and is expressed as (Van Genuchten 1980):

$$\theta = \theta_r + \frac{\theta_s - \theta_r}{[1+(\phi/\phi_m)^{\frac{1}{1-m}}]^m} \quad (1)$$

where θ is the volumetric water content; θ_r and θ_s denote the residual and saturated volumetric water content, respectively; $\phi = u_a - u_w$ is the matric suction, with u_a and u_w representing pore-air and pore water pressures; ϕ_m is the air-entry value; and *m* is an empirical fitting parameter of the SWCC.

Rewriting the Van Genuchten model in terms of effective saturation yields:

$$s_e = \frac{\theta - \theta_r}{\theta_s - \theta_r} = [1+(\phi/\phi_m)^{\frac{1}{1-m}}]^{-m} \quad (2)$$

where s_e is the effective saturation. Substituting Equation (2) into the statistical conductivity model proposed by Mualem (Mualem 1978) leads to the hydraulic conductivity function (HCF), which describes the variation of relative permeability and effective saturation:

$$k_r = s_e^{1/2}[1-(1-s_e^{1/m})^m]^2 \quad (3)$$

where k_r denotes the relative permeability. The hydraulic conductivity of unsaturated geomaterials can then be expressed as:

$$k = k_r \cdot k_s \quad (4)$$

where k_s is the saturated hydraulic conductivity. Combining Equations (3) and (4) yields the explicit form of the hydraulic conductivity function (HCF):

$$k = k_s s_e^{1/2}[1-(1-s_e^{1/m})^m]^2 \quad (5)$$

Equations (2) and (5) indicate that, during rainfall infiltration, the volumetric water content and effective saturation increase progressively, resulting in a reduction of matric suction and an increase in hydraulic conductivity. Once the geomaterials become fully saturated, matric suction drops to zero, and the hydraulic conductivity reaches its maximum value, k_s.

2.2. Shear strength of unsaturated geomaterials

The shear strength of saturated geomaterials is commonly described using the Mohr–Coulomb criterion, expressed as:

$$\tau = c' + (\sigma - u_w)\tan\varphi' \quad (6)$$

where τ is the shear strength of the geomaterial, c' is the effective cohesion, φ' is the effective friction angle, σ is the total stress, and $\sigma - u_w$ is the effective stress.

For unsaturated geomaterials, the presence of matric suction introduces capillary and bonding

effects between particles, which can enhance the shear strength of the soil to some extent. According to Fredlund and Morgenstern (Fredlund and Morgenstern 1977), the shear strength of unsaturated geomaterials can be expressed as:

$$\tau = c' = (\sigma - u_a)\tan\varphi' + (u_a - u_w)\tan\varphi_b \quad (7)$$

where φ_b is the friction angle associated matric suction, and $(u_a - u_w)\tan\varphi_b$ can be interpreted as the "apparent cohesion" contributed by the matric suction $u_a - u_w$. Under natural atmospheric conditions, when the geomaterial pores are in equilibrium with the atmosphere ($u_a = 0$), Equation (7) reduces to:

$$\tau = c' = \sigma\tan\varphi' - u_w\tan\varphi_b \quad (8)$$

Studies have shown that the relationship between matric suction and apparent cohesion is nonlinear. When matric suction is below the air-entry value ϕ_m, the geomaterial remains saturated and $\varphi_b = \varphi'$; when matric suction exceeds the residual suction ϕ_r, the geomaterial reaches the residual water content state, and $\varphi_b = 0$; when matric suction lies between the air-entry and residual suction values, φ_b decreases with increasing matric suction. Figure 1 illustrates the variation of apparent cohesion with matric suction, showing that apparent cohesion initially increases and then decreases, reaching a peak between the air-entry and residual suction values. At this peak, the shear strength of the geomaterial is maximized, and the slope is most stable (Cui et al. 2020).

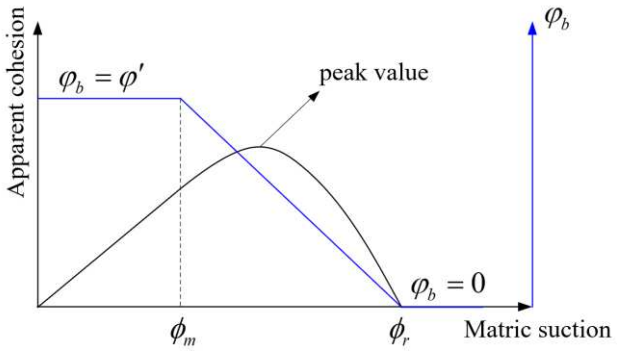


Fig. 1 Variation of apparent cohesion with matric suction (adapted from Cui et al. (Cui et al. 2020))

2.3. Strength reduction method

The strength reduction method (SRM) (Dawson et al. 1999) is a commonly used approach for calculating the FOS of slopes. The core idea of SRM is to progressively reduce the shear strength parameters of the geomaterial by a certain reduction factor during numerical analysis. When slope failure occurs in the simulation, the corresponding reduction factor is identified as the slope's FOS. Mathematically, the strength reduction is expressed as:

$$c_{\text{trial}} = c / F_{\text{trial}} \tag{9}$$

$$\varphi_{\text{trial}} = \arctan(\tan\varphi / F_{\text{trial}}) \tag{10}$$

where c and φ are the original cohesion and friction angle of the geomaterial, respectively; c_{trial} and φ_{trial} are the reduced strength parameters; F_{trial} is the reduction factor. In practice, F_{trial} is gradually increased until the numerical simulation exhibits signs of instability, such as non-convergence, formation of a through-going slip surface, or abrupt displacement increments. The corresponding reduction factor at this stage is taken as the FOS of slopes.

2.4. Slope failure probability and reliability index

The slope failure probability and reliability index are established based on the engineering limit state. According to the Unified Standard for Reliability Design of Engineering Structures (GB 50153-2008), the limit state of a slope can be described by the following limit state equation:

$$Z = g(X) = g(X_1, X_2, ..., X_n) = 0 \tag{11}$$

where $Z = g(\cdot)$ is the state function of the slope; $X_i (i = 1, 2, ..., n)$ represents the factors or random variables affecting slope stability, such as geotechnical parameters, rainfall events, groundwater level, rainfall conditions, blasting, or seismic loads. Macroscopically, these random variables can be classified into two integrated quantities: the resisting force *R* and the driving load *S*, leading to a simplified limit state equation:

$$R - S = 0 \tag{12}$$

The mean value and standard deviation of the slope state function *Z* are expressed as:

$$\mu_Z = \mu_R - \mu_S \tag{13}$$

$$\sigma_Z = \sqrt{\sigma_R^2 + \sigma_S^2} \tag{14}$$

It should be noted that the mean and standard deviation are only used to describe the statistical characteristics of the state function and cannot be directly used to calculate the reliability index. Although some studies calculate the reliability index using $\beta = \frac{\mu_Z}{\sigma_Z}$, this is based on the assumption that *Z* approximately follows a normal distribution (Chen 2018; Wu et al. 2019). Random variables affecting slope stability are physically non-negative, and their probability distributions are often modeled as lognormal. The difference of two lognormal variables, $Z = R - S$, does not have a closed-form analytical expression, making Monte Carlo simulation an effective tool to obtain the exact probability distribution. By generating a large number of random samples for R_i and S_i, $i = 1, 2, ..., N$, the state function samples are computed as $Z_i = R_i - S_i$. The slope failure probability is

then defined as the frequency of $Z_i \le 0$:

$$P_f = \frac{n_i\{Z_i \le 0\}}{N} \tag{15}$$

The reliability index β is related to the failure probability P_f as (GB 50153-2008):

$$\beta = -\Phi^{-1}(P_f) \tag{16}$$

where $\Phi^{-1}(\cdot)$ is the inverse of the standard normal cumulative distribution function.

3. Procedure for assessing the average maximum failure probability of unsaturated slopes over a given exposure period under stochastic rainfall

3.1. Concept of average maximum failure probability

Rainfall exhibits significant uncertainties in both spatial and temporal domains. For a given slope, assessing the failure probability under rainfall conditions requires a clear definition of the time scale (Lu et al. 2023). Suppose that, on average, *n* rainfall events occur within an exposure period *T* at the site of the slope. The slope stability is primarily controlled by the most critical rainfall event. The failure probability of the slope under rainfall conditions can be evaluated by defining the average maximum failure probability (AMFP). The calculation procedure is as follows:

(1) Establish uncertainty models of rainfall and geotechnical parameters based on historical rainfall data and site investigation data, respectively.

(2) Perform a Monte Carlo random sampling: randomly selecting *n* rainfall events and *m* geotechnical parameter sets from the respective models to obtain the rainfall event set $R = \{R_1, R_2, ...R_n\}$ and the geotechnical parameter set $M = \{M_1, M_2, ...M_m\}$.

(3) For a given rainfall event R_i ($1 \le i \le n$), compute the FOS of the slope for all *m* combinations of geotechnical parameters, and calculate the slope failure probability under rainfall R_i as p_i according to Equation (15). Denote the maximum failure probability among the *n* rainfall events as:

$$p_{\max} = \max(p_i) \tag{17}$$

(4) Repeat steps (2) and (3) for *l* times to ensure the stability of the Monte Carlo failure probability calculation. The AMFP $P_{f,T}$ and the reliability index β_T under *n* rainfall events within period *T* are then calculated using Equations (18) and (16):

$$P_{f,T} = \frac{1}{l}\sum_{j=1}^{l} p_{\max}^{j} \tag{18}$$

The proposed AMFP is not merely a statistical averaging procedure, but a time-exposure-oriented extreme risk metric for unsaturated slopes subjected to stochastic rainfall sequences. Within a given

exposure period T, slope instability is generally governed by the most adverse rainfall event rather than by average hydrological conditions. By explicitly incorporating the occurrence of multiple stochastic rainfall events and extracting the maximum failure probability among them, the AMFP captures the governing extreme scenario that controls slope safety. In probabilistic terms, AMFP represents the expected upper-bound failure likelihood conditioned on the occurrence of n rainfall events within T. It therefore transforms multi-event stochastic rainfall into a unified reliability indicator that is consistent with risk-based engineering decision-making. Compared with conventional single-event reliability analyses, the AMFP framework introduces a temporal aggregation mechanism that reflects cumulative exposure effects and extreme-event dominance. This enables a more realistic and conservative evaluation of slope safety in regions characterized by frequent or clustered rainfall events.

3.2. Surrogate modeling for efficient FOS evaluation in AMFP analysis

To compute $P_{f,T}$ and β_T, it is necessary to calculate FOS $n \times m \times l$ times. Since the Monte Carlo simulation parameters m and l are typically on the order of thousands or tens of thousands, relying solely on numerical simulation software for large-scale sampling and FOS calculation is highly inefficient. In recent years, surrogate models have been increasingly employed to replace computationally intensive and repetitive numerical simulations (Zhang et al. 2025; Zhuang et al. 2025). The general procedure for constructing a surrogate model is as follows: first, a certain number of samples are uniformly sampled from the data space of the random variables; second, compute FOS of each sample using numerical simulation; finally, the surrogate model is trained and subsequently used to predict the FOS for new input samples.

To establish the nonlinear mapping relationship between the uncertainties of rainfall and geotechnical parameters and the FOS of the slope, this study adopts the Support Vector Regression (SVR) model (Awad and Khanna 2015) as the surrogate model. As illustrated in Figure 2, SVR seeks an optimal regression hyperplane in a high-dimensional feature space, maximizing the fit of data within the ε-tube while minimizing model complexity. This allows for effective characterization of nonlinear relationships. SVR demonstrates good generalization ability under small-sample and low-dimensional feature conditions, can capture the complex nonlinear coupling between rainfall and geotechnical parameters, and shows robustness against outliers, making it well-suited for the surrogate modeling task in this study.

It should be noted that other models, such as multiple linear regression (Uyanık and Güler 2013), neural networks (Specht 1991), and random forests (Segal 2004), can also be employed for regression tasks. However, under the data conditions of this study, each of these methods has limitations. Multiple linear regression assumes a linear relationship between inputs and outputs, which makes it difficult to

capture the nonlinear coupling between rainfall and geotechnical parameters. Neural networks, although powerful for large-sample and high-dimensional problems, are prone to overfitting with a small sample size of approximately 1,000 and four features, and their performance is highly sensitive to network architecture and hyperparameters. Random forests have certain advantages in handling small-sample nonlinear problems, but SVR offers better parameter controllability, boundary smoothness, and stability in small-sample training, making it more suitable for this study. Considering model generalization, stability, and performance under small-sample conditions, SVR is selected as the optimal surrogate model to characterize the variations of FOS under multi-source uncertainty.

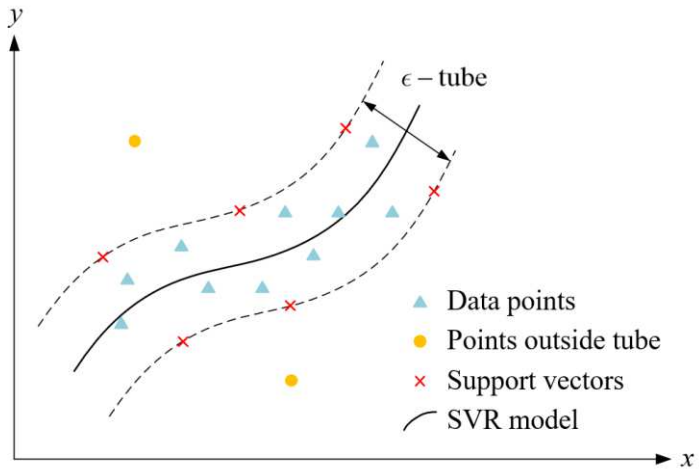


Fig. 2 Schematic diagram of Support Vector Regression (SVR) model

3.3. Overall framework and computational procedure

Figure 3 shows the overall framework for assessing the AMFP of unsaturated slopes over a given exposure period under stochastic rainfall. The framework integrates stochastic rainfall modeling, hydro-mechanical numerical simulation, surrogate modeling, and probabilistic aggregation into a unified exposure-period reliability assessment procedure. The detailed implementation of each step is described as follows.

Step (I) establishes the physical and geological basis of the study. A representative slope site is selected, and its geological, topographical, and hydrological conditions are characterized through field investigation and laboratory testing. Key geotechnical parameters, including cohesion, friction angle, unit weight, and unsaturated hydraulic properties, are determined to establish the physical basis for numerical modeling and probabilistic analysis.

Step (II) characterizes rainfall uncertainty. Historical hourly rainfall data are collected near the study site. The marginal distributions of rainfall duration and intensity are fitted using appropriate statistical models. A copula-based joint distribution (e.g., Frank Copula) is then established to capture their dependence structure, enabling stochastic generation of rainfall events consistent with historical observations.

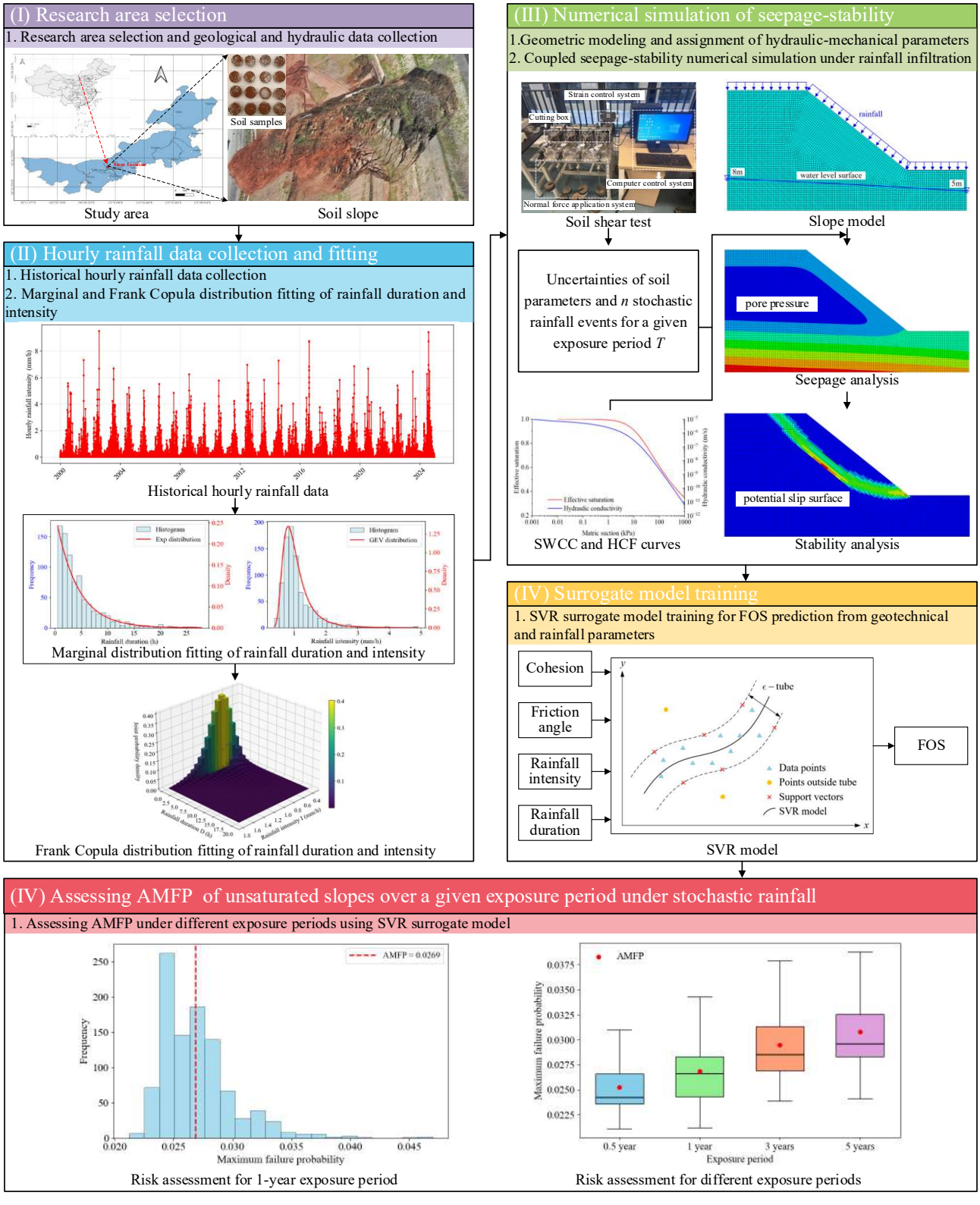


Fig. 3 Overall framework for assessing the AMFP of unsaturated slopes over a given exposure period under stochastic rainfall

Step (III) establishes the physical relationship between rainfall and slope stability. A coupled hydro-mechanical model is constructed to simulate transient seepage under rainfall infiltration. For each rainfall event and geotechnical parameter set, pore water pressure evolution is computed,

followed by slope stability analysis to obtain the FOS. This step establishes the mapping between stochastic inputs and slope stability responses.

Step (IV) improves computational efficiency. To reduce computational cost, a surrogate model (e.g., SVR) is trained to approximate the nonlinear relationship between rainfall characteristics, geotechnical parameters, and FOS. The validated surrogate replaces the numerical model in large-scale Monte Carlo simulations.

Step (V) performs exposure-period reliability aggregation, and its detailed computational procedure is illustrated in Figure 4. For a given exposure period T, the average number of rainfall events n is first determined. In each Monte Carlo realization (j=1, …, l), n rainfall events are randomly generated. For each rainfall event (i=1, …, n), m geotechnical parameter sets are sampled, and the surrogate model is used to predict FOS values and compute the corresponding failure probability p_i. After completing the inner loop, the maximum failure probability $p_{\max}$ within the exposure period is obtained. The outer Monte Carlo loop is repeated to ensure statistical stability, and the AMFP $P_{f,T}$ are finally calculated. This two-level looping structure converts multi-event stochastic rainfall into a unified exposure-period reliability metric.

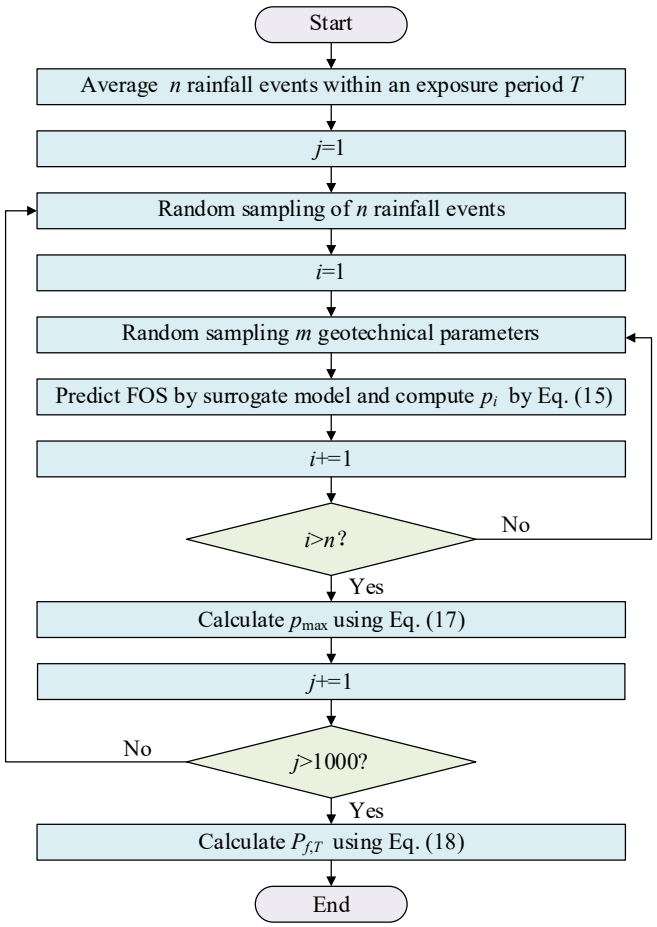


Fig. 4 Computational procedure of the AMFP

4. Case study

4.1. Study area and geotechnical uncertainty model

A homogeneous soil slope in the Baiyun-Obo mining area, Baotou, Inner Mongolia, China, is selected as the study object, and its location is shown in Figure 5. As illustrated in Figure 6, the slope geometry consists of a height of 30 m and an inclination angle of 38.7°. The water-head levels on the upstream and downstream sides are 8 m and 5 m, respectively, and the maximum matric suction reaches 50 kPa. The lateral boundaries of the model are impermeable and constrained in the horizontal direction; the bottom boundary is impermeable and constrained in both horizontal and vertical directions; the top boundary is subjected to rainfall infiltration. The soil is homogeneous and isotropic sandy loam and is modeled using the Mohr–Coulomb elastoplastic constitutive model; the corresponding parameters are listed in Table 1.

In general, soil parameters consist of two categories: strength parameters (Liao and Ji 2021; Nguyen and Likitlersuang 2019) (i.e., cohesion and friction angle) and hydraulic parameters (Dou et al. 2015; Zhang et al. 2025) (i.e., hydraulic conductivity, air-entry value, and SWCC parameters). However, strength parameters have been shown to exert a dominant influence on slope stability (Zhang et al. 2025). Therefore, to simplify the analysis, only the variability of strength parameters is considered in this study. Cohesion and friction angle are treated as random variables, and their coefficients of variation (0.15 and 0.10, respectively) are determined based on statistical analysis of laboratory test results. Considering the non-negativity of soil parameters from a physical perspective, the lognormal distribution is adopted as their probability model (Wu et al. 2018), that is:

$$\ln(X) \sim N(\mu_{\ln(X)}, \sigma^2_{\ln(X)}) .. \tag{19}$$

$$\mu_X = \exp(\mu_{\ln(X)} + \frac{1}{2}\sigma^2_{\ln(X)}) \tag{20}$$

$$\sigma_X = \sqrt{(\exp(\sigma^2_{\ln(X)}) - 1)\exp(2\mu_{\ln(X)} + \sigma^2_{\ln(X)})} \tag{21}$$

$$CV = \frac{\sigma_X}{\mu_X} = \sqrt{\exp(\sigma^2_{\ln(X)}) - 1} \tag{22}$$

where X denotes the random variable representing a geotechnical parameter; $\mu_{\ln(X)}$ and $\sigma_{\ln(X)}$ are the mean and standard deviation of $\ln X$, respectively; μ_X and σ_X are the mean and standard deviation of X, respectively; and CV denotes the coefficient of variation of X. Table 2 summarizes the probability distributions and statistical values of the random variables. Figure 7 presents the SWCC and HCF, which describe the dependence of effective saturation and hydraulic conductivity on matric suction, respectively, based on Equations (2) and (5).

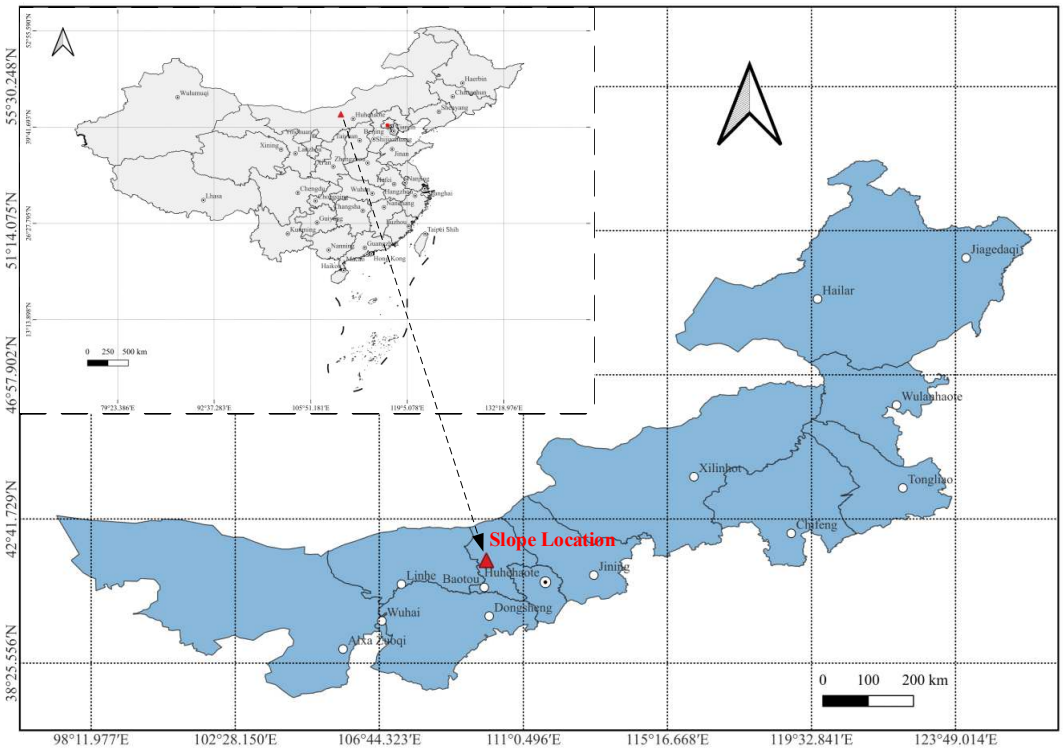


Fig. 5 Location of study slope

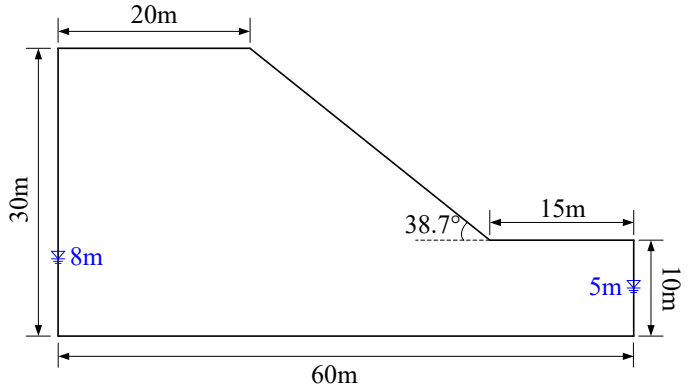


Fig. 6 The model of the study slope

Table 1 Parameters of unsaturated soil slope model

Parameter	Value
Cohesion c/(kPa)	8
Friction angle φ/(°)	24
Hydraulic conductivity k/(m·s^{-1})	1×10^{-5}
Air-entry value ϕ_m/(kPa)	15
Van Genuchten parameter m	0.20
Density ρ/(kg·m^{-3})	1800
Poisson's ratio υ	0.25
Elastic modulus E/(kPa)	20000
Porosity n	0.30

Table 2 Statistical properties and distributions of random variables

Parameter	Mean	Standard deviation	Distribution type	±3 times standard deviation range	±4 times *CV* range
ln*c*	2.0683	0.1492	Normal	5.06~12.37	3.2~12.8
ln*φ*	3.1731	0.0998	Normal	17.70~32.21	14~33

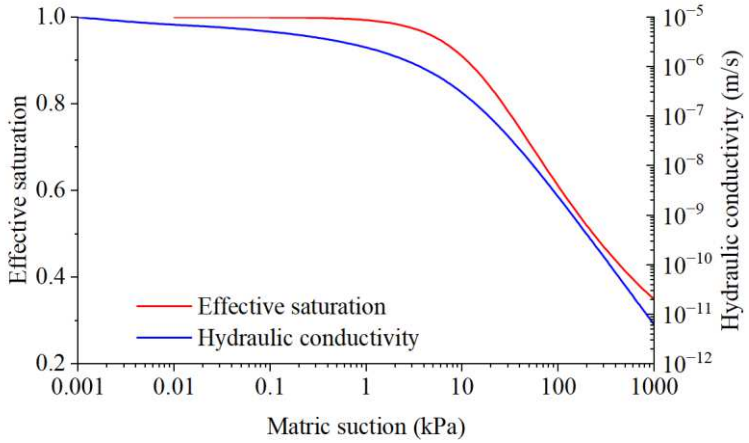
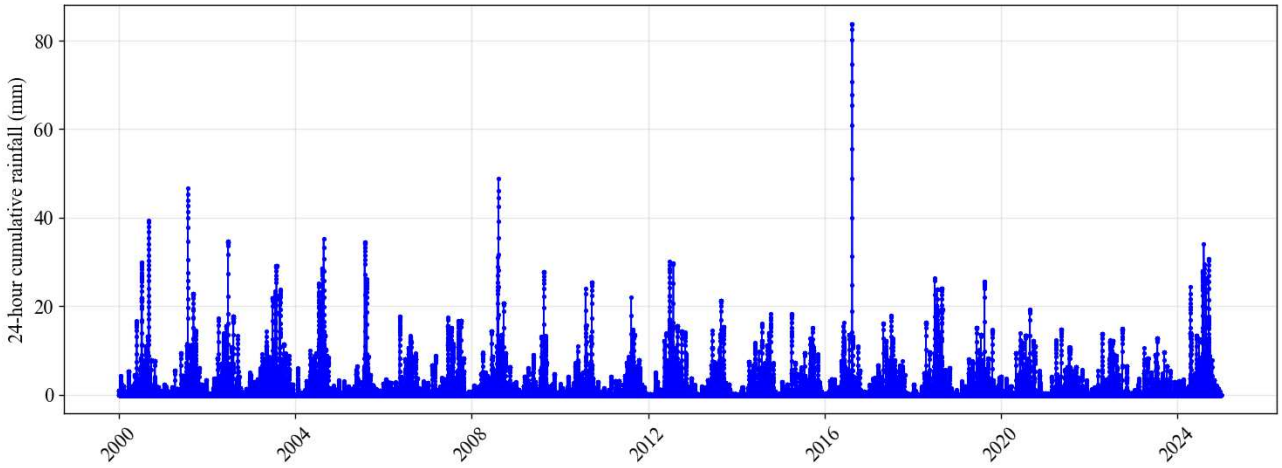


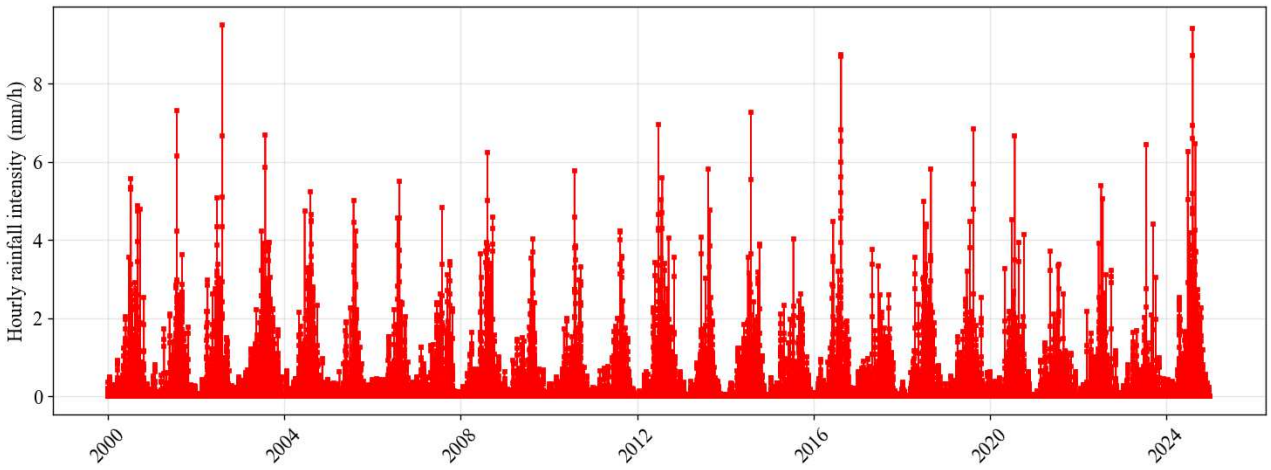
Fig. 7 Variations of effective saturation and hydraulic conductivity with matric suction

4.2. Calibration of the rainfall uncertainty model

Based on the latitude and longitude range of the Baiyun-Obo mining area in Baotou, the hourly rainfall data of the study area over the past 25 years (2000–2024) were obtained from the ERA5-Land dataset provided by the European Centre for Medium-Range Weather Forecasts (https://www.ecmwf.int). The ERA5-Land dataset provides global, high-resolution (0.1° × 0.1°) hourly climate data with high accuracy and consistency, making it suitable for regional rainfall analysis. As shown in Figure 8, the maximum 24-hour cumulative rainfall over the past 25 years does not exceed 84 mm, corresponding to “rainstorm” or lower levels according to the Grade of Precipitation (GB/T 28592-2012). The maximum hourly rainfall intensity is approximately 9.6 mm/h.



(a) 24-hour accumulative rainfall



(b) Hourly rainfall intensity

Fig. 8 Rainfall data in the study area from 2000 to 2024

Rainfall events $R=\{I,D\}$ can be characterized by two fundamental elements: rainfall intensity I and duration D (Liu and Wang 2024). The stability of a slope is influenced by both rainfall intensity and duration. Rainfall events are inherently uncertain. To obtain the probability distributions of rainfall intensity I and duration D, it is first necessary to define independent rainfall events from historical rainfall data. Considering that light rainfall events have little impact on slope stability, a rainfall intensity threshold (i) is initially set to filter out insignificant low-intensity rainfall. Independent rainfall events are then extracted using the Inter-Event Time Definition (IETD) (Adams et al. 1986). If the time interval between two rainfall segments exceeds the IETD, they are considered two independent rainfall events; otherwise, they are treated as a single event. Following the approach of Jun et al. (Jun et al. 2017), i and IETD are set to 0.5 mm/h and 9 h, respectively, yielding a total of 862 independent rainfall events, with an average of 34 events per year.

As shown in Figure 9, since the ERA5-Land dataset has an hourly resolution and rainfall data consist of discrete points, linear interpolation is applied to each independent rainfall event to obtain precise and continuous rainfall duration distributions. Rainfall intensity is then defined as the ratio of total rainfall V (mm) to rainfall duration D:

$$I=\frac{V}{D} \tag{23}$$

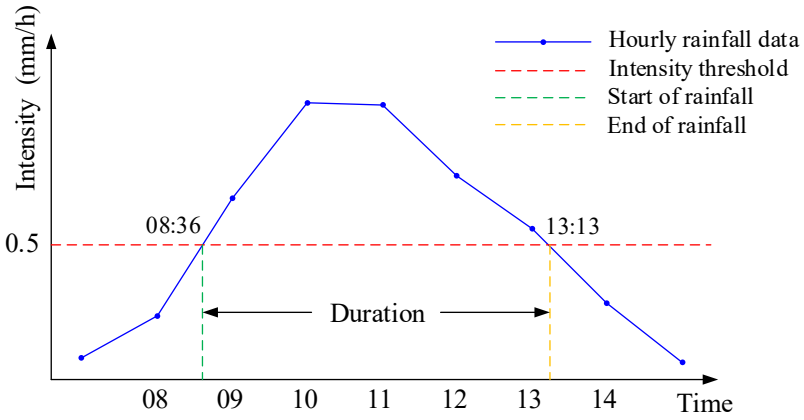


Fig. 9 Calculation of rainfall duration

Figure 10 shows the histograms of rainfall duration and rainfall intensity. Five candidate distribution models, including the Generalized Pareto Distribution (GPD), Lognormal Distribution (LogN), Normal Distribution (Normal), Exponential Distribution (Exp), and Generalized Extreme Value Distribution (GEV), were considered. The Maximum Likelihood Estimation (MLE) (Jun et al. 2017) was used to determine the optimal probability distributions for the two variables. The results indicate that rainfall duration D and rainfall intensity I follow the Exponential Distribution (Exp) and Generalized Extreme Value Distribution (GEV), respectively, as shown in Figure 10. Their probability density functions (PDFs) are given in Equations (24) and (25), and the distribution parameters are listed in Table 3.

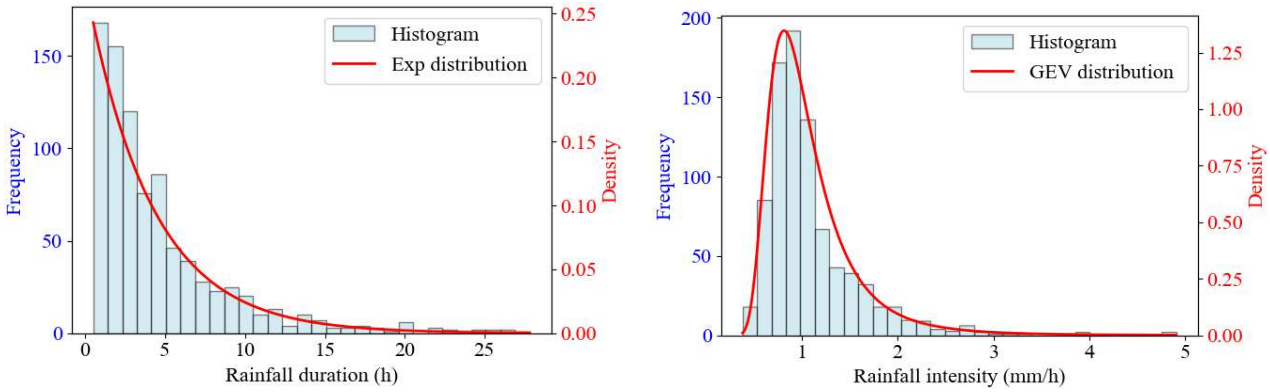
$$f(D)=\frac{1}{\sigma}\exp(-\frac{D-\mu}{\sigma}) \tag{24}$$

$$f(I)=\frac{1}{\sigma}[1+\xi(\frac{I-\mu}{\sigma})]^{-(1+\frac{1}{\xi})}\exp\left\{-[1+\xi(\frac{I-\mu}{\sigma})]^{-\frac{1}{\xi}}\right\} \tag{25}$$

where μ, σ and ξ are the location, scale, and shape parameters, respectively. The cumulative distribution functions (CDFs) corresponding to the Exponential Distribution (Exp) and the Generalized Extreme Value Distribution (GEV) are:

$$F(D)=1-\exp(-\frac{D-\mu}{\sigma}) \tag{26}$$

$$F(I)=\exp\left\{-[1+\xi(\frac{I-\mu}{\sigma})]^{-\frac{1}{\xi}}\right\} \tag{27}$$



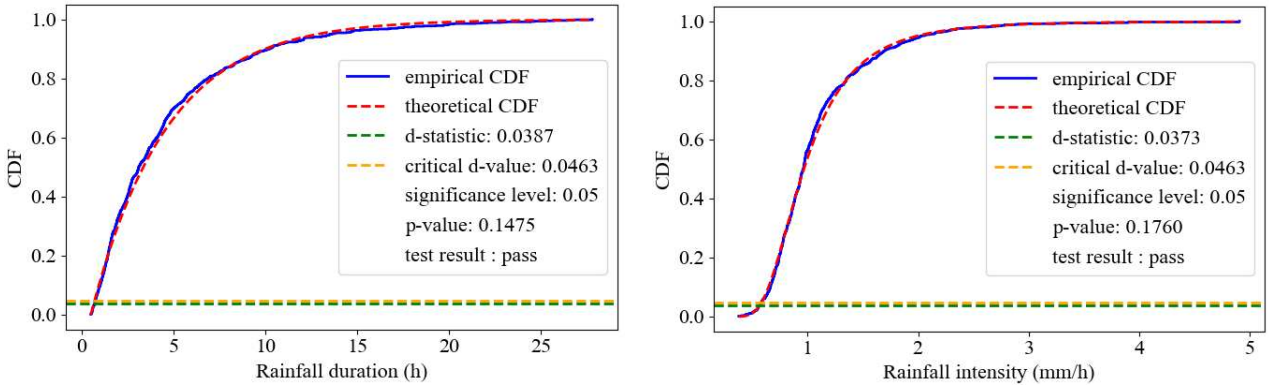
(a) Rainfall duration (b) Rainfall intensity

Fig. 10 Histograms and probability density functions (PDFs) of rainfall duration and rainfall intensity

Table 3 Parameters of the optimal distribution models

Variable	Optimal distribution	μ	σ	ξ	θ
Rainfall duration D	Exponential	0.500	4.114	/	
Rainfall intensity I	Generalized Extreme Value	0.862	0.278	-0.199	
	Frank Copula parameter				2.579

To statistically validate the suitability of the Exponential Distribution (Exp) and the Generalized Extreme Value Distribution (GEV) as the optimal marginal distributions for rainfall duration and intensity, the Kolmogorov–Smirnov (K–S) test (Berger and Zhou 2014) was further employed to assess the goodness of fit. The test assumes that the sample follows the above theoretical distribution and evaluates the fit by calculating the maximum difference (the d-statistic) between the empirical cumulative distribution function and the theoretical cumulative distribution function. As shown in Figure 11 and Table 4, the K–S test results indicate that the empirical and theoretical cumulative distribution curves are in good agreement. At a significance level of 0.05, the p-values are all greater than 0.05 and the d-statistics are all below the critical values; therefore, the null hypothesis is not rejected, confirming that the selected distribution models provide a good fit to the observed data.



(a) Rainfall duration (b) Rainfall intensity

Fig. 11 Comparison of empirical and theoretical cumulative distribution functions (CDFs)

Table 4 K-S test results

Variable	Distribution type	Sample number	Significance level	p-value	Critical d-value	d-statistic
Rainfall duration D	Exponential	862	0.05	0.1475	0.0463	0.0387
Rainfall intensity I	Generalized Extreme Value	862	0.05	0.1760	0.0463	0.0373

The above approach defines the uncertainties of rainfall duration and rainfall intensity separately using individual marginal distribution models. However, rainfall duration and intensity often exhibit a certain degree of dependence. The Frank copula function (Jun et al. 2017; J. Zhang et al. 2025) is employed to construct the bivariate joint cumulative distribution function of rainfall duration and intensity:

$$C(F(I),F(D),\theta)=-\frac{1}{\theta}\ln[1+\frac{(e^{-\theta F(I)}-1)(e^{-\theta F(D)}-1)}{e^{-\theta}-1}] \tag{28}$$

where θ is the Frank copula parameter; $C(F(I),F(D),\theta)$ represents the probability that rainfall intensity is less than I and rainfall duration is less than D. The Frank copula parameter θ can be estimated using the Maximum Likelihood Estimation (MLE) or the method of moments based on Kendall's rank correlation coefficient τ. The following analytical relationship exists between θ and τ (Nelsen 2006):

$$\tau=1-\frac{4}{\theta}[1-\frac{1}{\theta}\int_0^{\theta}\frac{t}{e^t-1}dt] \tag{29}$$

This study employs a dual verification mechanism to ensure the accuracy of the estimated Frank copula parameter θ. First, the parameter is primarily estimated using the Maximum Likelihood Estimation (MLE) method, yielding $\theta=2.579$. Second, the theoretical Kendall's rank correlation coefficient, $\tau_{\text{theory}}=0.269$, is computed using Equation (29). Finally, the Kendall's rank correlation coefficient, $\tau_{\text{sample}}=0.262$, is directly calculated from the samples according to Equation (30) (Kendall 1938).

$$\tau_{\text{sample}}=\frac{2}{n(n-1)}\sum_{i<j}\text{sgn}[(D_i-D_j)(I_i-I_j)] \tag{30}$$

where n denotes the sample size. The close agreement between τ_{theory} and τ_{sample} indicates that the Frank copula parameter, $\theta=2.579$, estimated by MLE accurately captures the dependence between rainfall duration and intensity. Figure 12 presents the histogram of the joint probability density distribution of rainfall duration and intensity. The joint probability distribution constructed based on

copula theory maintains strict consistency with the specified marginal distributions, fully preserving the core statistical characteristics of the original data.

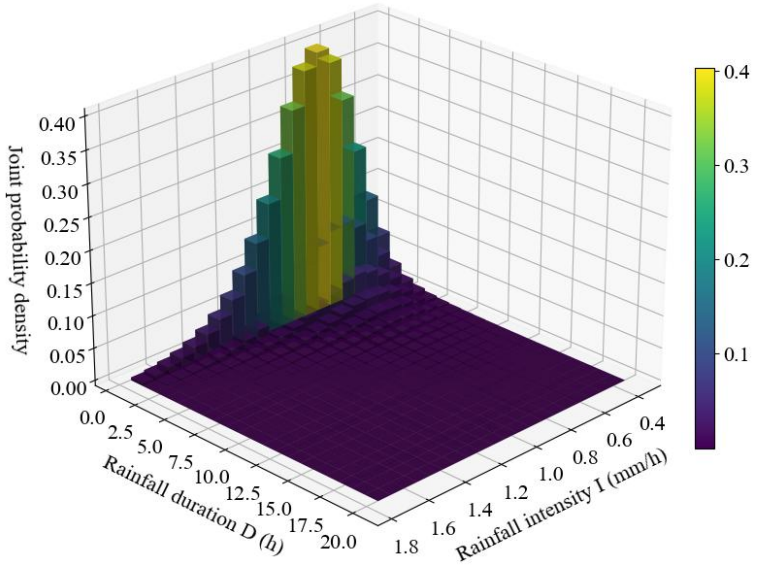


Fig. 12 Histogram of the joint probability density distribution of rainfall duration and intensity

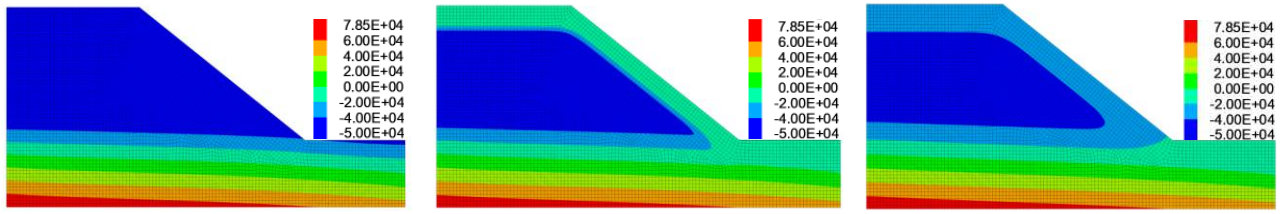
4.3. Numerical validation of unsaturated hydro-mechanical coupling simulation

Implementation of unsaturated seepage in FLAC3D requires secondary development using the FISH script, and the approach proposed by Jiang et al. (Jiang et al. 2014) provides a very useful reference. In this study, the FLAC3D unsaturated hydro-mechanical coupling program was first compiled using FISH and then embedded into a self-developed sample iterative calculation module. The FLAC3D model adopts a hexahedral brick-shaped mesh with eight vertices, featuring a thickness of 0.5 m along the Y-axis and a uniform element size of 0.5 m, totaling 5,128 volumetric elements. To verify the accuracy of the unsaturated hydro-mechanical coupling numerical program, the simulation responses were examined under three different scenarios: scenario 1 considers suction but no rainfall, with ϕ=-50kPa and R=0; scenario 2 considers suction with short-duration intense rainfall, ϕ=-50 kPa and R=240 mm/2d; and scenario 3 involves suction with long-duration weak rainfall, ϕ=-50 kPa and R=96 mm/20d.

The pore water pressure and saturation under the three different scenarios are shown in Figure 13 and Figure 14, respectively. Figure 15 presents the contour of maximum shear strain increment, with the maximum shear strain increment zone indicating the location and shape of the potential most critical slip surface. In scenario 1, the soil above the water table exhibits matric suction, with a maximum suction of 50 kPa. For soil with matric suction exceeding the air-entry value, pores begin to drain, placing the soil above the water table in an unsaturated state. According to the Van Genuchten model established in Equation (2), the minimum saturation of the soil is 0.711. The slope remains stable, with a FOS of 1.184. In scenario 2, short-duration intense rainfall rapidly brings the surface soil

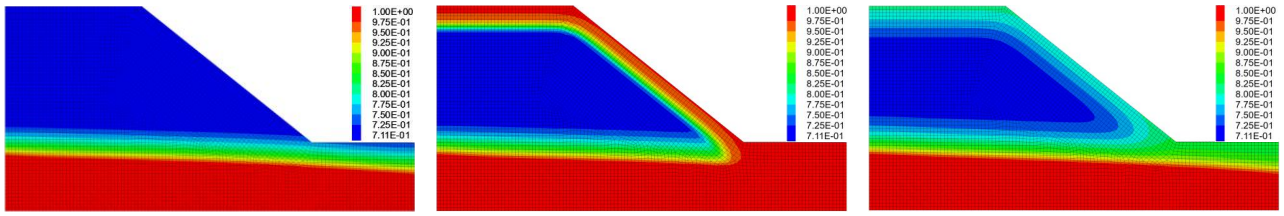
near saturation, increases surface soil permeability, and accelerates the downward propagation of the wetting front, significantly reducing the effect of matric suction. The slip surface occurs within the saturated zone, and the FOS decreases to 1.015. In contrast, the weak rainfall intensity in Scenario 3 only slightly increases the water content in the shallow soil, and the overall effect is limited. No saturated zone forms at the slope surface, surface soil permeability remains low, and the wetting front descends slowly, so the effect of matric suction is only slightly reduced. The potential slip surface remains deep, similar to that in scenario 1, with a corresponding FOS of 1.152.

These numerical simulation results indicate that short-duration intense rainfall tends to induce shallow sliding, and long-duration weak rainfall may trigger deeper instability. These findings are consistent with existing research, confirming the accuracy of the unsaturated hydro-mechanical coupling numerical model.



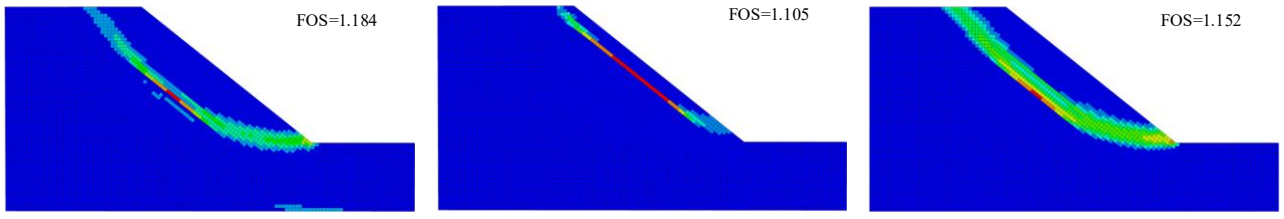
(a) Scenario 1 (b) Scenario 2 (c) Scenario 3

Fig. 13 Contour of pore water pressure



(a) Scenario 1 (b) Scenario 2 (c) Scenario 3

Fig. 14 Contour of saturation



(a) Scenario 1 (b) Scenario 2 (c) Scenario 3

Fig. 15 Potential slip surface geometry and corresponding FOS

4.4. Training and evaluation of the surrogate model

In this study, rainfall duration, rainfall intensity, cohesion, and friction angle are four key uncertain variables affecting slope stability. According to Figure 10, the main ranges of rainfall duration and intensity are 0.5~28 h and 0.5~5 mm/h, respectively. A total of 1000 input samples were generated by randomly sampling these four variables. Rainfall duration and intensity were uniformly

sampled within their respective ranges, while cohesion and friction angle were uniformly sampled within ±4 times *CV* range around the mean values. The corresponding FOS for each sample was computed using FLAC3D, resulting in 1000 input–output pairs for surrogate model training.

The dataset was randomly split into 70% for training and 30% for testing. The training set was used for model fitting, while the test set was used for final performance evaluation. During training, grid search was conducted to optimize the SVR hyperparameters (penalty coefficient C, tolerance ò, and Radial Basis Function kernel parameter γ), resulting in the optimal combination: C=1000, ò =0.01, γ=0.01. Using these optimal parameters, 10-fold cross-validation was performed on the training set to evaluate model stability. The results showed an average root mean square error (RMSE) of 0.0194 with a standard deviation of 0.0022, indicating stable fitting without significant error fluctuations.

Performance evaluation on the test set included three typical metrics: (1) coefficient of determination R^2, measuring goodness of fit; (2) RMSE, reflecting the square mean of prediction deviations; and (3) mean absolute error (MAE), indicating the average magnitude of prediction errors. Figure 16 shows the scatter plot of predicted versus true FOS values. The SVR model fits the data very well, with R^2=0.9997, RMSE=0.0047, and MAE=0.0036. These results demonstrate that the surrogate model achieves extremely high accuracy in predicting FOS and can effectively replace complex numerical computations.

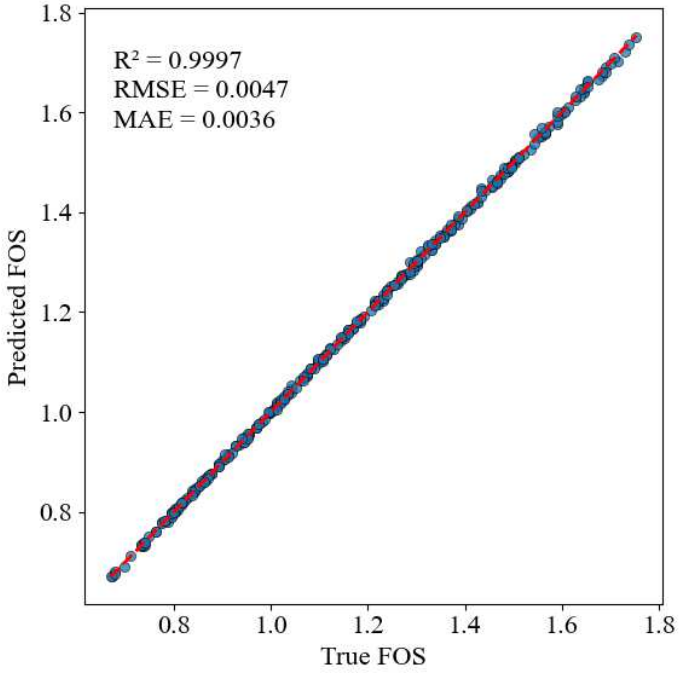
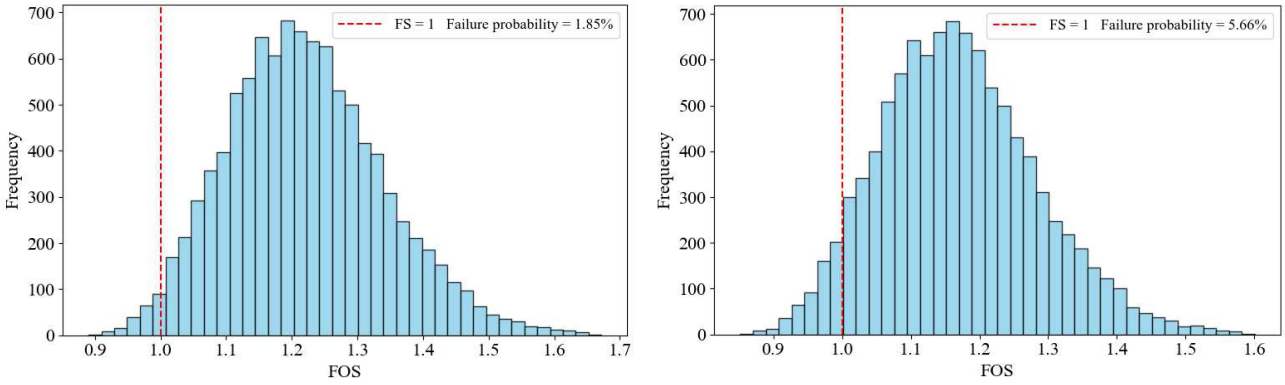


Fig. 16 Scatter plot of predicted versus true FOS values

4.5. Calculation of AMFP

Assuming an analysis period of one year, the annual AMFP under multiple rainfall events are

evaluated. A total of 10000 sets of geotechnical parameters are generated using Monte Carlo simulation. To ensure that the sampled parameters remain within the valid domain of the surrogate model, the Monte Carlo sampling is conducted within the ±3 times standard deviation range of the lognormal distributions of the geotechnical parameters. First, the slope failure probability under historical minimum rainfall (D=0.5 h, I=0.5 mm/h, regarded as no rainfall) and historical maximum rainfall (D=28 h, I=5 mm/h) was analyzed. As shown in Figure 17, under no rainfall, the slope failure probability and reliability index are 1.85% and 2.086, respectively, with a mean FOS of 1.220. Under the historical maximum rainfall, the failure probability and reliability index are 5.66% and 1.584, respectively, with a mean FOS of 1.169.



(a) No rainfall (b) Historical maximum rainfall

Fig. 17 Slope failure probability under no rainfall and historical maximum rainfall

According to Section 4.2, the study area experiences an average of 34 rainfall events per year. Based on the constructed Frank Copula distribution model of rainfall, 34 rainfall events were randomly sampled to calculate the maximum failure probability. This sampling process was repeated 1,000 times. Figure 18 presents the histogram of the maximum failure probability, which mainly falls within the range of 2.15%–4.65%, with an AMFP of 2.69% and a standard deviation of 0.0033. The corresponding reliability index calculated according to Equation (16) is 1.927.

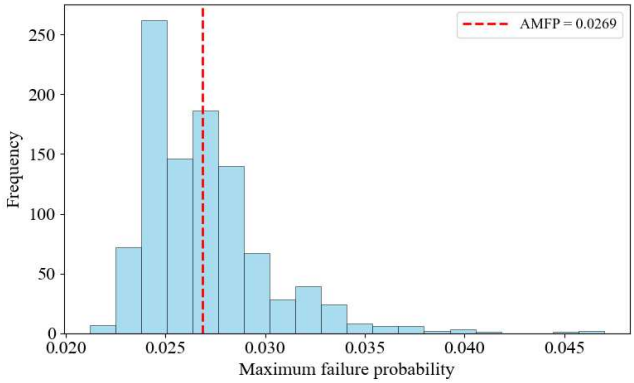


Fig. 18 Distribution of maximum failure probability for an exposure period of 1 year

Figure 19 presents the boxplots of the maximum failure probability under different exposure

periods. The AMFP increases monotonically with exposure period, rising from 0.0252 for T=0.5 year to 0.0269 for 1 year, 0.0295 for 3 years, and 0.0308 for 5 years. This gradual upward trend clearly indicates cumulative risk amplification under stochastic rainfall. Both the median and the interquartile range shift upward as the exposure period increases, suggesting that not only the expected failure probability but also its variability becomes larger over time. This behavior is consistent with extreme-value theory, as longer exposure periods increase the likelihood of encountering more critical rainfall events, thereby elevating the maximum failure probability within the considered period.

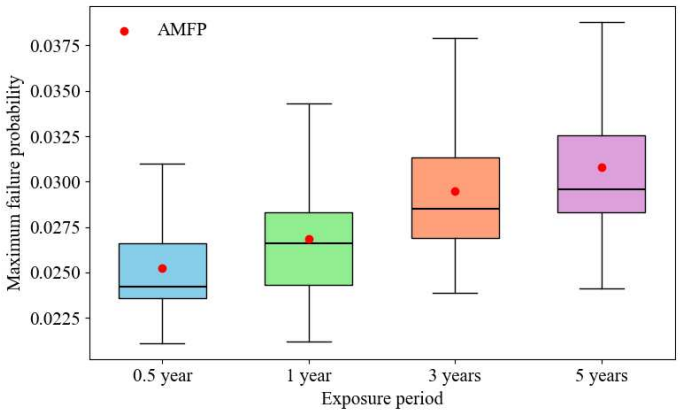


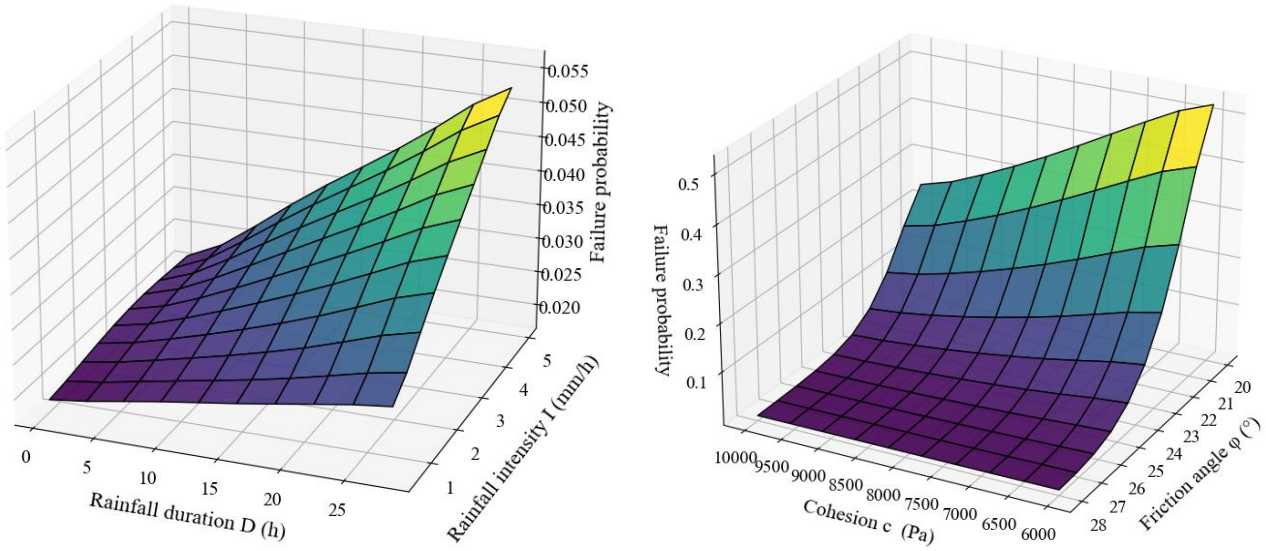
Fig. 19 Boxplots of the maximum failure probability under different exposure periods

5. Discussion

5.1. Sensitivity analysis of slope failure probability

This study further investigated the sensitivity of slope failure probability to rainfall and soil parameters. Uniform sampling was conducted over the ranges of rainfall duration (0.5~28 h) and rainfall intensity (0.5~5 mm/h), and the slope failure probability under different rainfall conditions was computed to generate a 3D fragility surface, as shown in Figure 20a. The failure probability increases along both the rainfall duration and rainfall intensity axes at comparable rates, indicating that rainfall duration and rainfall intensity exert similarly significant influences on slope stability. Therefore, in slope safety management and disaster early warning, equal attention should be paid to both long-duration rainfall events and high-intensity rainfall events.

For a fixed rainfall event (D=5 h, I=2 mm/h), the mean values of cohesion and friction angle were varied within certain ranges to compute the slope failure probability 3D fragility surface under the given rainfall condition, as illustrated in Figure 20b. The increase in failure probability along the friction angle direction is significantly greater than that along the cohesion direction, suggesting that slope stability is more strongly influenced by the friction angle. Moreover, the slope failure probability is more sensitive to changes in soil parameters, indicating that although rainfall can reduce slope stability to some extent, its influence is far less significant than that of soil strength parameters, which remain the dominant factor controlling slope stability under rainfall conditions.

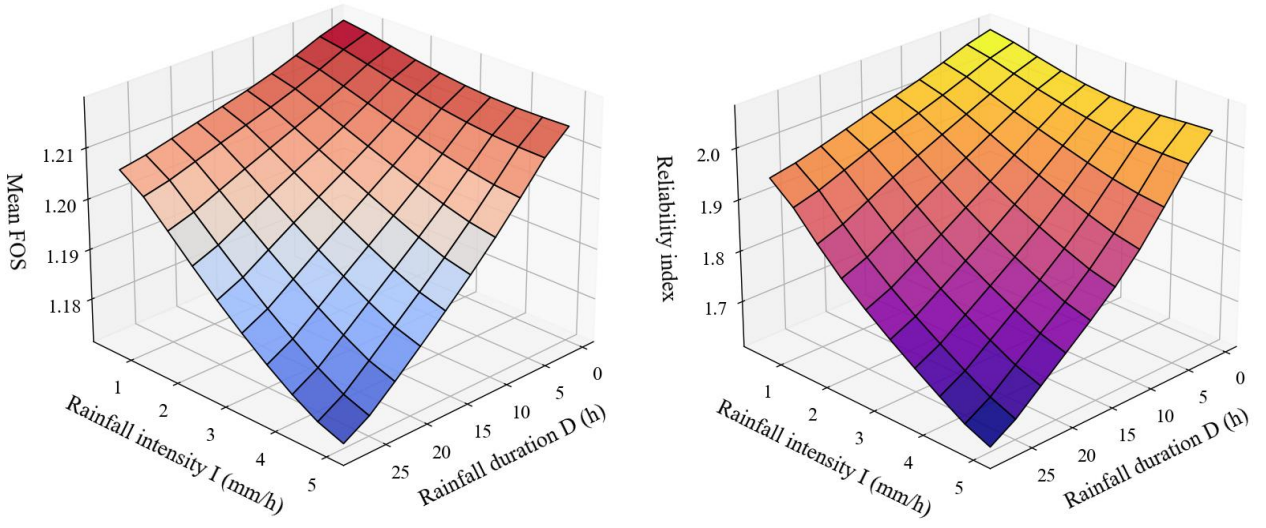


(a) Rainfall parameters (b) Soil parameters

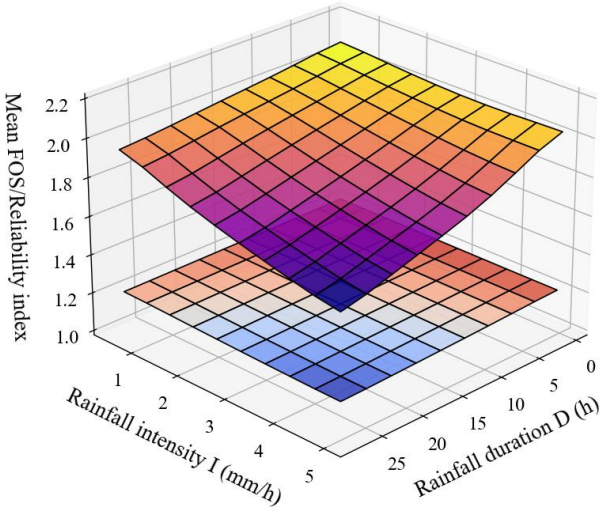
Fig. 20 Sensitivity analysis of failure probability

5.2. Comparison of rainfall sensitivity in mean FOS and reliability index

This section compares the sensitivity of the mean FOS and the reliability index to rainfall variations, as mentioned in Section 4.5. The mean FOS is a deterministic evaluation metric, suitable for quickly assessing the overall stability of a slope. In contrast, the reliability index is based on the probabilistic principle of failure probability and can quantify the evolution of slope instability risk under rainfall. As shown in Figure 21, under varying rainfall conditions, the mean FOS ranges from 1.169 to 1.220, whereas the reliability index varies from 1.584 to 2.086. This indicates that the reliability index is more sensitive to rainfall perturbations and can more accurately reflect changes in slope stability, providing a more reliable basis for slope risk assessment and the establishment of early-warning thresholds.



(a) Mean FOS (b) Reliability index



(c) FOS and reliability index

Fig. 21 Rainfall sensitivity comparison of mean FOS and reliability index

5.3. Computational efficiency analysis

All computations in this study were performed on a desktop computer with an Intel(R) Core(TM) i5-12600KF processor. The majority of the computational time was consumed in calculating FOS for 1000 samples using FLAC. Unlike software that relies on graphical user interfaces for interactive modeling and computation (e.g., GeoStudio), FLAC, as a command-driven numerical analysis software, allows users to implement automated sample iteration via FISH scripting, thus eliminating manual parameter updating.

It should be noted that FLAC calculates FOS using the strength reduction method (SRM), which is slightly slower than limit equilibrium method. With a mesh size of 0.5 m, the computation for a single sample takes approximately 50 s, resulting in a total of about 13.8 h for 1000 sample iterations. Although the overall computational burden may seem substantial, the surrogate model itself is trained in about 1 minute, and then it requires only 0.1 s to evaluate 34×10000 samples. If the analysis fully relied on FLAC-based numerical simulations, performing 10000 realizations would require approximately 5.8 days, which corresponds to only a single Monte Carlo sampling process. Taking the annual average of 34 rainfall events used in this study as an example, a traditional numerical approach would demand 34×10000×1000 simulations, which is practically infeasible. In contrast, the SVR-based surrogate model requires only 56 minutes to complete the same computations, thereby achieving a substantial improvement in computational efficiency and feasibility.

5.4. Applicability analysis of the method

The method proposed in this study is based on the mechanical response of unsaturated slopes under rainfall infiltration, with a core focus on the influence of matric suction (negative pore water pressure) on slope stability. Therefore, it is highly applicable to soil slopes and unsaturated slopes

containing weak interlayers. The model can effectively capture the changes in pore water pressure induced by rainfall infiltration and their impact on slope failure probability, providing direct insights into slope shear strength, potential slip surface development, and failure risk assessment.

For compact rock slopes, due to their extremely low porosity, the concept of matric suction (negative pore water pressure) is theoretically inapplicable. However, in fractured or weathered rock masses, negative pore water pressure effects similar to matric suction may develop locally, which can still influence local stability. Therefore, the proposed method is primarily applicable to non-saturated feature analysis in localized zones such as fractures or weathered layers of rock slopes, and it is not suitable for evaluating the overall stability of intact, compact rock masses.

6. Conclusions

This study developed a probabilistic framework for assessing the average maximum failure probability (AMFP) of unsaturated slopes over a given exposure period T under multiple stochastic rainfall events. By explicitly incorporating rainfall randomness, geotechnical uncertainty, and unsaturated hydro–mechanical coupling, the proposed framework enables time-dependent reliability evaluation based on the cumulative effect of sequential rainfall events. The proposed method is publicly available at https://github.com/fddpx/RainfallInfiltrationSlopeAnalysis. The main findings are summarized as follows:

(1) A joint probability model of rainfall duration and intensity was established using the Frank Copula (θ=2.579) based on 25 years of historical rainfall data. The adopted exponential and generalized extreme value distributions effectively captured the long-tail characteristics of extreme rainfall events. This probabilistic rainfall model provides the statistical foundation for evaluating AMFP over a specified exposure period.

(2) Unsaturated seepage–stability coupling simulations were implemented in FLAC3D using customized FISH scripts. Numerical simulations indicate that short-duration, high-intensity rainfall predominantly induces shallow failures, whereas long-duration, low-intensity rainfall tends to trigger deep-seated failures. These distinct failure mechanisms explain how different rainfall patterns contribute to the maximum failure probability governing AMFP.

(3) A Support Vector Regression (SVR) surrogate model was constructed to efficiently predict the factor of safety (FOS), achieving high predictive accuracy (R^2=0.9997, RMSE=0.0047, MAE=0.0036). By replacing repeated numerical simulations, the surrogate model enables large-scale Monte Carlo sampling required for robust AMFP estimation while significantly reducing computational cost.

(4) The AMFP exhibits a clear monotonic increase with exposure duration. Specifically, the AMFP increases from 0.0252 (T=0.5 year) to 0.0269 (1 year), 0.0295 (3 years), and 0.0308 (5 years),

demonstrating cumulative amplification of failure risk under stochastic rainfall. The upward shift in both central tendency and dispersion confirms that longer exposure periods increase not only the expected maximum failure probability but also the likelihood of encountering critical rainfall events. This finding quantitatively demonstrates the exposure-time effect in rainfall-induced slope reliability.

Overall, the AMFP-based framework provides a theoretically consistent and computationally efficient methodology for time-dependent slope reliability assessment. By linking stochastic rainfall occurrence with exposure-period-based extreme response, the proposed approach bridges the gap between single-event stability evaluation and long-term probabilistic risk management. Compared with the conventional factor of safety (FOS), the reliability index derived from AMFP exhibits higher sensitivity to rainfall-induced variations in failure probability, making it more suitable for quantitative risk assessment, engineering design, hazard mitigation, and early-warning threshold formulation.

CRediT authorship contribution statement

Beibei Sun: Conceptualization, Data curation, Methodology, Writing – original draft. **Shunchuan Wu:** Conceptualization, Supervision, Writing – review & editing. **Longqiang Han:** Methodology, Supervision, Funding acquisition, Writing – original draft. **Qiang Zhu:** Validation, Visualization, Writing – review & editing. **Chaoqun Chu:** Validation.

Declaration of competing interest

The authors declare that they have no known competing financial interests or personal relationships that could have appeared to influence the work reported in this paper.

Acknowledgements

This research was supported by National Natural Science Foundation of China 42302313，Yunnan Provincial Department of Education Key Industry Science and Technology Project for University Services FWCY-QYCT2024009，Young Talents Project of “Xingdian Talent Support Program” in Yunnan Province KKXX202521023

Data availability

Our code has been publicly released at the following platform: https://github.com/fddpx/RainfallInfiltrationSlopeAnalysis. Researchers are welcome to modify, further develop, and deploy it according to their specific needs.

References

Adams B J, Fraser H G, Howard C D D, Hanafy M S (1986) Meteorological data analysis for drainage system design. Journal of Environmental Engineering (United States) 112(5):827-848. http://doi.org/10.1061/(ASCE)0733-9372(1986)112:5(827)

Alsubal S, Sapari N B, Harahap I S H, Ali Mohammed Al-Bared M (2019) A review on mechanism of rainwater in triggering landslide. Iop Conference Series: Materials Science and Engineering 513(1):12009. http://doi.org/10.1088/1757-899X/513/1/012009

Awad M, Khanna R. (2015). Support vector regression, in: fficient learning machines: Theories, concepts, and applications for engineers and system designers. Springer, pp 67–80. https://doi.org/10.1007/978-1-4302-5990-9_4

Bai H, Feng W, Li S, Ye L, Wu Z, Hu R, Dai H, Hu Y, Yi X, Deng P (2022) Flow-slide characteristics and failure mechanism of shallow landslides in granite residual soil under heavy rainfall. J Mt Sci-Engl 19(6):1541-1557. http://doi.org/10.1007/s11629-022-7315-8

Berger V W, Zhou Y (2014) Kolmogorov–smirnov test: Overview. Wiley Statsref: Statistics Reference Online

Chen Z Y (2018) Reliability analysis and safety criterion in geotechnical engineering based on the index of safety margin. Chin J Rock Mech Eng 37(03):521-544. http://doi.org/10.13722/j.cnki.jrme.2017.1302

Cui P B, Zhu Y Q, Liu Y, Wang Q L, Pan Y D (2020) Calculation of ultimate supporting forces of shield tunnels in unsaturated sandy soils considering soil arching effects. Chin J Geotech Eng 42(05):873-881. http://doi.org/10.11779/CJGE202005009

Dawson E M, Roth W H, Drescher A (1999) Slope stability analysis by strength reduction. Geotechnique 49(6):835-840. https://doi.org/10.1680/geot.1999.49.6.835

Dou H, Han T, Gong X, Qiu Z, Li Z (2015) Effects of the spatial variability of permeability on rainfall-induced landslides. Eng Geol 192:92-100. https://doi.org/10.1016/j.enggeo.2015.03.014

Fang H, Wu Y, Qu C, Lin Y (2024) Investigation of topographic amplification on ground motions considering spatial variability of soil properties. Stoch Env Res Risk A 38(3):901-922. http://doi.org/10.1007/s00477-023-02605-y

Fredlund D G. (2021). Use of soil–water characteristic curves in the implementation of unsaturated soil mechanics, in: Unsaturated Soils-Volume 3. CRC Press, Boca Raton, pp 887–902.

Fredlund D G, Morgenstern N R (1977) Stress state variables for unsaturated soils. Journal of the Geotechnical Engineering Division 103(5):447-466. https://doi.org/10.1061/AJGEB6.0000720

GB 50153-2008, 2008. Unified Standard for Reliability Design of Engineering Structures. China Architecture and Building Press, Beijing.

GB/T 28592-2012, 2012. Grade of Precipitation. Standards press of China, Beijing.

Haque U, Blum P, Da Silva P F, Andersen P, Pilz J, Chalov S R, Malet J, Auflič M J, Andres N, Poyiadji E, Lamas P C, Zhang W, Peshevski I, Pétursson H G, Kurt T, Dobrev N, García-Davalillo J C, Halkia M, Ferri S, Gaprindashvili G, Engström J, Keellings D (2016) Fatal landslides in Europe. Landslides 13(6):1545-1554. http://doi.org/10.1007/s10346-016-0689-3

Jiang S, Li D, Zhang L, Zhou C (2014) Slope reliability analysis considering spatially variable shear strength parameters using a non-intrusive stochastic finite element method. Eng Geol 168:120-128. https://doi.org/10.1016/j.enggeo.2013.11.006

Jiang Z M, Xiong X H, Zeng L (2014) Unsaturated seepage analysis of slope under rainfall condition based on FLAC^{3D}. Rock Soil Mech 35(03):855-861. http://doi.org/10.16285/j.rsm.2014.03.016

Jun C, Qin X, Gan T Y, Tung Y, De Michele C (2017) Bivariate frequency analysis of rainfall intensity and duration for urban stormwater infrastructure design. J Hydrol 553:374-383. http://doi.org/10.1016/j.jhydrol.2017.08.004

Kendall M G (1938) A new measure of rank correlation. Biometrika 30(1-2):81-93. https://doi.org/10.1093/BIOMET/30.1-2.81

Li L, Wang Y, Cao Z, Chu X (2013) Risk de-aggregation and system reliability analysis of slope stability using representative slip surfaces. Comput Geotech 53:95-105. https://doi.org/10.1016/j.compgeo.2013.05.004

Liao W, Ji J (2021) Time-dependent reliability analysis of rainfall-induced shallow landslides considering spatial variability of soil permeability. Comput Geotech 129:103903. https://doi.org/10.1016/j.compgeo.2020.103903

Liu X, Wang Y (2021) Reliability analysis of an existing slope at a specific site considering rainfall triggering mechanism and its past performance records. Eng Geol 288:106144. https://doi.org/10.1016/j.enggeo.2021.106144

Liu X, Wang Y (2023) Probabilistic hazard analysis of rainfall-induced landslides at a specific slope considering rainfall uncertainty and soil spatial variability. Comput Geotech 162:105706. https://doi.org/10.1016/j.compgeo.2023.105706

Liu X, Wang Y (2024) Quantifying impacts of precipitation scenarios projected under climate change on annual probability of rainfall-induced landslides at a specific slope. Comput Geotech 167:106063. https://doi.org/10.1016/j.compgeo.2023.106063

Liu Y, Deng Z, Wang X (2021) The effects of rainfall, soil type and slope on the processes and mechanisms of rainfall-induced shallow landslides. Applied Sciences 11(24):11652. https://doi.org/10.3390/app112411652

Lu M, Zheng J, Zhang J, Huang H (2023) On assessing the probability of rainfall-induced slope failure during a given exposure time. Acta Geotech 18(3):1255-1267. http://doi.org/10.1007/s11440-022-01655-w

Ma J Z, Zhang J, Huang H W, Zhang L L, Huang J S (2017) Identification of representative slip surfaces for reliability analysis of soil slopes based on shear strength reduction. Comput Geotech 85:199-206. https://doi.org/10.1016/j.compgeo.2016.12.033

Mualem Y (1978) Hydraulic conductivity of unsaturated porous media: generalized macroscopic approach. Water Resour Res 14(2):325-334. https://doi.org/10.1029/WR014i002p00325

Nelsen R B. (2006). An Introduction to Copulas, 2nd ed. Springer, New York. https://doi.org/10.1007/0-387-28678-0

Nguyen T S, Likitlersuang S (2019) Reliability analysis of unsaturated soil slope stability under infiltration considering hydraulic and shear strength parameters. B Eng Geol Environ 78(8):5727-5743. http://doi.org/10.1007/s10064-019-01513-2

Ran Q, Hong Y, Li W, Gao J (2018) A modelling study of rainfall-induced shallow landslide mechanisms under different rainfall characteristics. J Hydrol 563:790-801. https://doi.org/10.1016/j.jhydrol.2018.06.040

Reale C, Xue J, Pan Z, Gavin K (2015) Deterministic and probabilistic multi-modal analysis of slope stability. Comput Geotech 66:172-179. https://doi.org/10.1016/j.compgeo.2015.01.017

Segal M R (2004) Machine Learning Benchmarks and Random Forest Regression. Center for Bioinformatics and Molecular Biostatistics.

Shi Z N, Qi S X, Fu H Q, Zeng L, He Z M, Fang R M (2020) A study of water content distribution and shallow stability of earth slopes subject to rainfall infiltration. Rock Soil Mech 41(03):980-988. http://doi.org/10.16285/j.rsm.2019.0474

Specht D F (1991) A general regression neural network. IEEE Transactions on Neural Networks 2(6):568-576. https://doi.org/10.1109/72.97934

Tang G, Huang J, Sheng D, Sloan S W (2018) Stability analysis of unsaturated soil slopes under random rainfall patterns. Eng Geol 245:322-332. https://doi.org/10.1016/j.enggeo.2018.09.013

Uyanık G K, Güler N (2013) A study on multiple linear regression analysis. Procedia-Social and Behavioral Sciences 106:234-240. https://doi.org/10.1016/j.sbspro.2013.12.027

765 Van Genuchten M T (1980) A closed-form equation for predicting the hydraulic conductivity of unsaturated soils.
766 Soil Sci Soc Am J 44(5):892-898. https://doi.org/10.2136/sssaj 1980.03615995004400050002x
767 Wang B, Vardon P J, Hicks M A (2018) Rainfall-induced slope collapse with coupled material point method. Eng
768 Geol 239:1-12. https://doi.org/10.1016/j.enggeo.2018.02.007
769 Wang J, Xu W (2025) Slope stability and failure dynamics of rainfall-induced landslide: Algorithm and applications.
770 Comput Geotech 177:106919. http://doi.org/10.1016/j.compgeo.2024.106919
771 Wu F, Zhang L L, Zheng W T, Wei X (2018) Probabilistic back analysis method for unsaturated soil slopes with
772 fluid-solid coupling process based on polynomial chaos expansion. Chin J Geotech Eng 40(12):2215-2222.
773 http://doi.org/10.11779/CJGE201812008
774 Wu S C, Shi W B, Han L Q (2024) Slope Engineering 2nd ed. Metallurgical Industry Press, Beijing.
775 Wu S C, Zhang H J, Xiao S, Han L Q (2019) Study on time-varying target reliability of open-pit slope considering
776 service life. J Min Saf Eng 36(03):542-548. http://doi.org/10.13545/j.cnki.jmse.2019.03.015
777 Yan T, Xiong J, Ye L, Gao J, Xu H (2023) Field investigation and finite element analysis of landslide-triggering
778 factors of a cut slope composed of granite residual soil: a case study of Chongtou town, Lishui city, China.
779 Sustainability 15(8):6999. http://doi.org/10.3390/su15086999
780 Yazdi J S, Moss R E S (2025) Soil Slope reliability assessment through bayesian updating: a comparative study using
781 RLEM, RFDM, and RFEM. Int J Geomech 25(2):4024338. http://doi.org/10.1061/IJGNAI.GMENG-1021
782 Zhang J, Tao Y Y, Lu M, Yan Z X R (2025) An efficient method for calculating annual probability of rainfall-induced
783 slope failure. J Tongji Univ (Nat Sci) 53(08):1207-1217. http://doi.org/10.11908/j.issn.0253-374x.24057
784 Zhang J, Yang B, Lu M, Sharma A (2025) Assessing annual failure probability of soil slopes under rainfall and
785 evaporation. Comput Geotech 187:107517. http://doi.org/10.1016/j.compgeo.2025.107517
786 Zhang Q, Xu Q, Yi J S, Xu L, Ma Z G (2016) Rainfall infiltration depth and formation mechanism of slow-inclination
787 soil landslides in Nanjiang. Chin J Geotech Eng 38(08):1447-1455. https://doi.org/ 10.11779/CJGE201608012
788 Zhang Z, Wu S, Han L, He P, Ren M (2025) Risk estimation for earth slopes with multiple failure modes based on
789 the generalized subset simulation. Stoch Env Res Risk A 39:5919-5931 http://doi.org/10.1007/s00477-025-
790 03097-8
791 Zhou Z, Shen J, Li Y, Duan W, Yang R, Shu J, Li H, Tao S, Zheng S (2021) Mechanism of colluvial landslide
792 induction by rainfall and slope construction: A case study. J Mt Sci-Engl 18(4):1013-1033.
793 http://doi.org/10.1007/s11629-020-6048-9
794 Zhuang W, Liu Y, Zhang K, Lyu Q, Hou S, Yang Q (2025) A physics knowledge-based surrogate model framework
795 for time-dependent slope deformation: Considering water effect and sliding states. J Rock Mech Geotech
796 17(9):5416-5436. http://doi.org/10.1016/j.jrmge.2024.11.002
797